

Received 24 January; accepted 28 May 2003; doi:10.1038/nature01774.

- Hertz, J. A. Quantum critical phenomena. *Phys. Rev. B* **14**, 1165–1184 (1976).
- Millis, A. J. Effect of a nonzero temperature on quantum critical points in itinerant fermion systems. *Phys. Rev. B* **48**, 7183–7196 (1993).
- Continentino, M. A. Quantum scaling in many-body systems. *Phys. Rep.* **239**, 179–213 (1994).
- Si, Q., Rabello, S., Ingersent, K. & Smith, J. L. Locally critical quantum phase transitions in strongly correlated metals. *Nature* **413**, 804–808 (2001).
- Coleman, P. & Pépin, C. What is the fate of the heavy electron at a quantum critical point? *Physica B* **312**, 383–389 (2002).
- Gegenwart, P. *et al.* Magnetic-field induced quantum critical point in YbRh₂Si₂. *Phys. Rev. Lett.* **89**, 056402 (2002).
- Heuser, K. *et al.* Inducement of non-Fermi-liquid behavior with a magnetic field. *Phys. Rev. B* **57**, R4198–R4201 (1998).
- Stockert, O. *et al.* Pressure versus magnetic-field tuning of a magnetic quantum phase transition. *Physica B* **312–313**, 458–460 (2002).
- Trovarelli, O. *et al.* YbRh₂Si₂: Pronounced non-Fermi-liquid effects above a low-lying magnetic phase transition. *Phys. Rev. Lett.* **85**, 626–629 (2000).
- Kadowaki, K. & Woods, S. B. Universal relationship of the resistivity and specific heat in heavy-fermion compounds. *Solid State Commun.* **58**, 507–509 (1986).
- Gegenwart, P. *et al.* Divergence of the heavy quasiparticle mass at the antiferromagnetic quantum critical point in YbRh₂Si₂. *Acta Phys. Pol. B* **34**, 323–334 (2003).
- Landau, L. D. The theory of a Fermi liquid. *Sov. Phys. JETP* **3**, 920–925 (1957).
- Paul, I. & Kotliar, G. Thermoelectric behavior near the magnetic quantum critical point. *Phys. Rev. B* **64**, 184414 (2001).
- Giamarchi, T., Varma, C. M., Ruckenstein, A. E. & Nozières, P. Singular low energy properties of an impurity model with finite range interactions. *Phys. Rev. Lett.* **70**, 3967–3970 (1993).
- Schröder, A. *et al.* Onset of antiferromagnetism in heavy-fermion metals. *Nature* **407**, 351–355 (2000).
- Mederle, S. *et al.* Unconventional metallic state in YbRh₂(Si_{1-x}Ge_x)₂—a high pressure study. *J. Phys. Condens. Matter* **14**, 10731–10736 (2002).
- Plessel, J. *et al.* Unusual behavior of the low-moment magnetic ground-state of YbRh₂Si₂ under high pressure. *Phys. Rev. B* **67**, 180303 (2003).
- Francois, M., Venturini, G., Marchéché, J. F., Malaman, B. & Roques, B. De Nouvelles séries de germaniures, isotopes de U₁Re₃Si₆, ThCr₂Si₂ et CaBe₂Ge₂, dans les systèmes ternaires R-T-Ge où R est un élément des terres rares et T = Ru, Os, Rh, Ir: supraconductivité de LaIr₂Ge₂. *J. Less Common Metals* **113**, 231–237 (1985).
- Carter, G. C., *et al.* in *Metallic shifts in NMR*. *Progress in Materials Science* Vol. 20, Part I, Ch. 9 (eds Chalmers, B., Christian, J. W. & Massalski, T. B.) 123–124 (Oxford, Pergamon, 1977).

Acknowledgements We acknowledge discussions with J. Ferstl, C. Langhammer, S. Mederle, N. Oeschler, I. Zerec, G. Sparn, O. Stockert, M. Abd-Elmeguid, J. Hopkinson, A. I. Larkin and I. Paul. Work at Dresden is partially supported by the Fonds der Chemischen Industrie and by the FERLIN project of the European Science Foundation. P. C. is supported by the National Science Foundation. Y. T. is a Young Scientist Research Fellow supported by the Japan Society for the Promotion of Science.

Competing interests statement The authors declare that they have no competing financial interests.

Correspondence and requests for materials should be addressed to P.C. (coleman@physics.rutgers.edu).

Superconductivity phase diagram of Na_xCoO₂·1.3H₂O

R. E. Schaak¹, T. Klimczuk^{1,2}, M. L. Foo¹ & R. J. Cava^{1,3}

¹Department of Chemistry, Princeton University, Princeton, New Jersey 08544, USA

²Faculty of Applied Physics and Mathematics, Gdansk University of Technology, Narutowicza 11/12, 80-952 Gdansk, Poland

³Princeton Materials Institute, Princeton University, Princeton, New Jersey 08540, USA

The microscopic origin of superconductivity in the high-transition-temperature (high-*T_c*) copper oxides remains the subject of active inquiry; several of their electronic characteristics are well established as universal to all the known materials, forming the experimental foundation that all theories must address. The most fundamental of those characteristics, for both the copper oxides and other superconductors, is the dependence of the superconducting *T_c* on the degree of electronic band filling. The recent report of superconductivity¹ near 4 K in the layered sodium cobalt oxyhydrate, Na_{0.35}CoO₂·1.3H₂O, is of interest

owing to both its triangular cobalt–oxygen lattice and its generally analogous chemical and structural relationships to the copper oxide superconductors. Here we show that the superconducting *T_c* of this compound displays the same kind of behaviour on chemical doping that is observed in the high-*T_c* copper oxides. Specifically, the optimal superconducting *T_c* occurs in a narrow range of sodium concentrations (and therefore electron concentrations) and decreases for both underdoped and overdoped materials, as observed in the phase diagram of the copper oxide superconductors. The analogy is not perfect, however, suggesting that Na_xCoO₂·1.3H₂O, with its triangular lattice geometry and special magnetic characteristics, may provide insights into systems where coupled charge and spin dynamics play an essential role in leading to superconductivity.

Like the high-*T_c* superconductors, the Na_xCoO₂·1.3H₂O crystal structure¹ consists of electronically active planes (in this case, edge-sharing CoO₆ octahedra) separated by layers (in this case, Na_x·1.3H₂O) that act as spacers, to yield electronic two-dimensionality, and also act as charge reservoirs (see below). We have found that varying the Na content in Na_xCoO₂·1.3H₂O results in the same type of out-of-plane chemical doping control of in-plane electronic

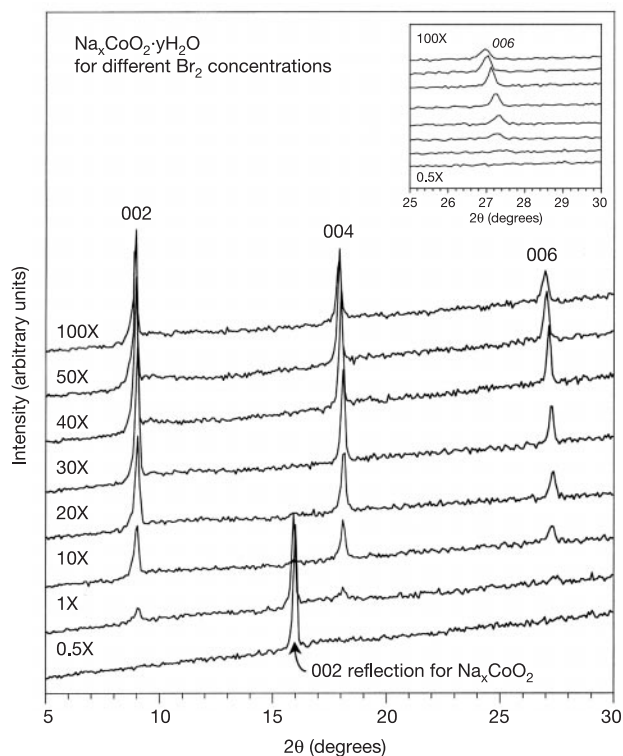


Figure 1 Powder X-ray diffraction patterns (Cu K α radiation) for Na_xCoO₂·yH₂O samples prepared using different concentrations of the bromine de-intercalant. Inset, an enlargement of the 006 reflections for each sample, highlighting the shift in the layer spacing as a function of sodium content. The Na_xCoO₂·yH₂O samples were prepared by chemically de-intercalating sodium from Na_{0.7}CoO₂ using bromine as an oxidizing agent. Na_{0.7}CoO₂ (0.5 g) was stirred in 20 ml of a Br₂ solution in acetonitrile at room temperature for five days. Bromine concentrations representing substoichiometric (0.5 \times), stoichiometric (1 \times), and molar excess (10–100 \times) relative to sodium content were employed. ('1 \times ' indicates that the amount of Br₂ used is exactly the amount that would theoretically be needed to remove all of the sodium from Na_{0.7}CoO₂). The product was washed several times with acetonitrile and then water, and then dried briefly under ambient conditions. The sodium content of the phases was determined by the inductively coupled plasma atomic emission spectroscopy (ICP-AES) method. Very high Na diffusion coefficients facilitate homogenization of the Na contents of the samples at ambient temperature.

charge that is found for the copper oxide superconductors. This is achieved by changing the Br concentration used in the de-intercalation of the host material. (See Fig. 1 legend for the synthesis procedure). Powder X-ray diffraction (XRD) patterns for the synthesized samples are shown in Fig. 1. The bromine-treated samples made with substoichiometric (0.5x; see Fig. 1 legend for definition of this nomenclature) and stoichiometric (1x) bromine solutions consist primarily of a partially de-intercalated, anhydrous, non-superconducting Na_xCoO_2 phase ($c \approx 11.2 \text{ \AA}$). A small amount of the hydrated superconducting phase $\text{Na}_x\text{CoO}_2 \cdot 1.3\text{H}_2\text{O}$ ($c \approx 19.6 \text{ \AA}$) is detectable by XRD for the 1x sample. Single phase, superconducting, fully hydrated $\text{Na}_x\text{CoO}_2 \cdot 1.3\text{H}_2\text{O}$ occurs for higher Br concentrations, with a small amount of Na_xCoO_2 in the 10x sample. Chemical analysis indicates that the sodium content of the resulting materials generally varies systematically in the samples prepared in different Br concentrations, over a range of $x = 0.26$ to 0.45 (Table 1).

Thermogravimetric analysis of all the samples on very slow heating in oxygen (Fig. 2 inset) showed that their behaviour was identical to that reported previously for $\text{Na}_{0.3}\text{CoO}_2 \cdot y\text{H}_2\text{O}$ (ref. 2). The interlayer 'crystal water' content remains essentially constant, at approximately 1.3 per formula unit, despite differences in sodium content in the single phase samples. The intergrain water is variable from sample to sample, as is to be expected. Figure 1 shows a noticeable shift in the positions of the 001 reflections for the fully hydrated $\text{Na}_x\text{CoO}_2 \cdot 1.3\text{H}_2\text{O}$ phases, yielding a systematic variation in the c axes of the unit cells (Table 1) from 19.43 Å for the $x = 0.45$ sample to 19.77 Å for the $x = 0.26$ sample. This increase in layer separation with decreasing sodium content for the hydrated superconducting phase is similar to that observed in the dehydrated Na_xCoO_2 phase^{3,4}. The a axis, reflecting the in-plane CoO_6 dimensions, is independent of Na content within the precision of our measurements.

Zero field cooled d.c. magnetization data measured in a field of 5 Oe for selected samples are shown in the main panel of Fig. 2. The magnetizations at 1.8 K represent approximately 100% of the theoretical value expected for perfect diamagnetism. Such strong diamagnetic signals provide evidence for bulk superconductivity. Na concentration inhomogeneities in the samples are probably the primary source of rounding of the superconducting transitions. An important point revealed by the data in Fig. 2 is that T_c for each sample is clearly different, indicating that differences in sodium content significantly affect the superconductivity of $\text{Na}_x\text{CoO}_2 \cdot 1.3\text{H}_2\text{O}$.

In order to characterize fully the dependence of T_c on sodium content, we used a.c. susceptibility, which is more sensitive to weakly superconducting samples. Figure 3 shows the a.c. susceptibility for all the $\text{Na}_x\text{CoO}_2 \cdot y\text{H}_2\text{O}$ samples. For the multiple phase $x = 0.45$ and $x = 0.40$ samples, the T_c values are approximately 2.0 K (Table 1), and the diamagnetic a.c. signals are very small,

Table 1 Characterization of $\text{Na}_x\text{CoO}_2 \cdot y\text{H}_2\text{O}$

Sodium content* (x in $\text{Na}_x\text{CoO}_2 \cdot y\text{H}_2\text{O}$)	Bromine concentration	a axis of $\text{Na}_x\text{CoO}_2 \cdot y\text{H}_2\text{O}^\dagger$ (Å)	c axis of $\text{Na}_x\text{CoO}_2 \cdot y\text{H}_2\text{O}^\dagger$ (Å)	$T_c \ddagger$ (K)
0.45	0.5 x	N/A	N/A	2.0
0.40	1 x	2.823(3)	19.43(2)	2.0
0.32	10 x	2.825(2)	19.52(2)	2.1
0.33	20 x	2.823(2)	19.58(1)	2.2
0.32	30 x	2.822(2)	19.58(1)	3.0
0.30	40 x	2.823(2)	19.69(2)	4.3
0.29	100 x	2.819(3)	19.77(2)	4.0
0.26	50 x	2.821(2)	19.77(2)	2.4

$\text{Na}_x\text{CoO}_2 \cdot y\text{H}_2\text{O}$ was prepared by bromine de-intercalation and hydration of $\text{Na}_{0.7}\text{CoO}_2$.

* Sodium content determined by ICP-AES. The estimated error of analysis is ± 0.02 per formula unit.

† Determined by least squares refinement of powder XRD data, from 6–10 reflections between 2θ values of 5° and 60° .

‡ T_c s determined from the a.c. susceptibility data, from the extrapolation of the steepest slope of the M versus T curves in Fig. 3 to $M = 0$.

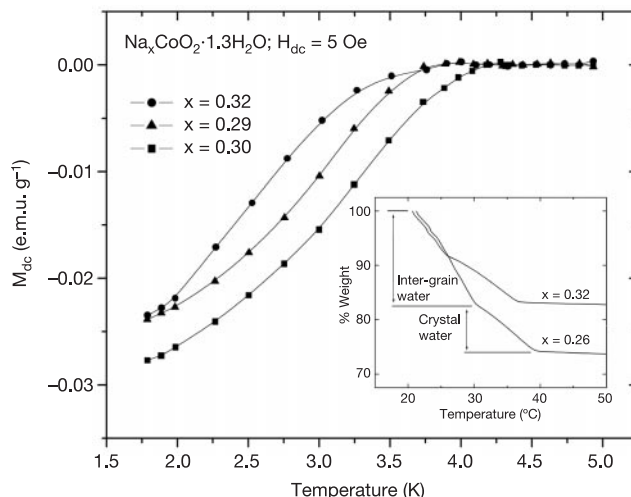


Figure 2 Zero field cooled d.c. magnetization for superconducting samples of $\text{Na}_x\text{CoO}_2 \cdot 1.3\text{H}_2\text{O}$. Data were obtained for $x = 0.29, 0.30$ and 0.32 , using a Quantum Design PPMS magnetometer, $H_{dc} = 5 \text{ Oe}$. Inset, loss in weight of single phase $\text{Na}_x\text{CoO}_2 \cdot 1.3\text{H}_2\text{O}$ ($x = 0.26$ and 0.32) samples heated extremely slowly in O_2 (0.25 degrees per minute) illustrating the method by which we distinguish the amount of crystal water (the higher-temperature weight loss) from the intergrain water (the lower-temperature weight loss). The change in weight that occurs on loss of crystal water is seen to be essentially the same in both low-Na and high-Na content materials.

consistent with their phase analysis by XRD, which shows primarily non-superconducting, anhydrous Na_xCoO_2 . In the $x = 0.40$ sample, the fully hydrated $\text{Na}_x\text{CoO}_2 \cdot 1.3\text{H}_2\text{O}$ phase accounts for approximately 15% of the sample, allowing us to estimate the maximum sodium content of the $\text{Na}_x\text{CoO}_2 \cdot 1.3\text{H}_2\text{O}$ phase to be approximately $x = 0.35$. The data suggest that at its highest possible Na content, the $\text{Na}_x\text{CoO}_2 \cdot 1.3\text{H}_2\text{O}$ phase has a T_c near 2 K.

All other samples are single phase sodium cobalt oxyhydrate with the crystal structure of the superconductor. The $x = 0.32$ and $x = 0.33$ samples yield slightly higher T_c values (between 2.1 and 2.2 K) and signals that are one to two orders of magnitude higher than the multiple phase $x = 0.40$ sample. Single phase samples with sodium contents of $x = 0.32, 0.30$ and 0.29 display superconducting

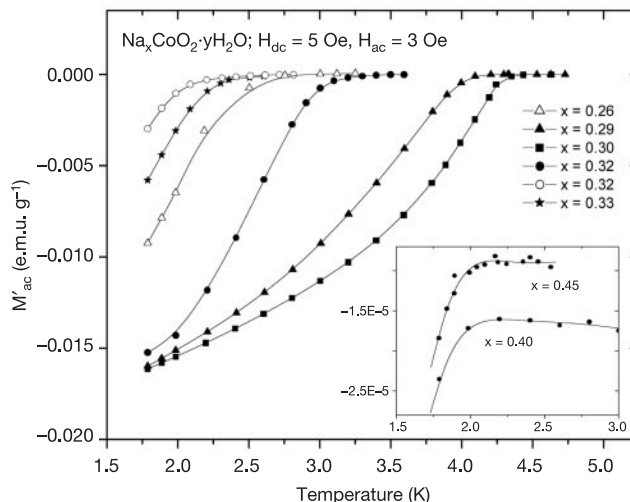


Figure 3 Zero-field cooled a.c. magnetization for all superconducting $\text{Na}_x\text{CoO}_2 \cdot y\text{H}_2\text{O}$ samples. ($H_{dc} = 3 \text{ Oe}$, $H_{ac} = 5 \text{ Oe}$, $f = 10 \text{ kHz}$) Magnetization data for the weakly superconducting samples $x = 0.45$ and 0.40 are shown in the inset.

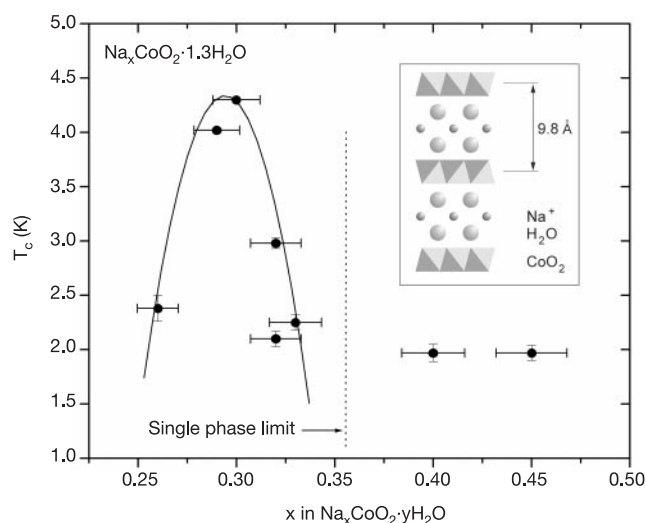


Figure 4 The superconducting phase diagram for $\text{Na}_x\text{CoO}_2 \cdot 1.3\text{H}_2\text{O}$. Main panel, T_c as a function of x as determined from the a.c. susceptibility measurements in Fig. 3. Inset, schematic representation of the layered crystal structure of $\text{Na}_x\text{CoO}_2 \cdot 1.3\text{H}_2\text{O}$. Triangular layers of CoO_6 edge-shared octahedra are shown in a polyhedral representation.

T_c values of 3.0 K, 4.3 K and 4.0 K, respectively (Fig. 3). Significantly, the single phase sample with $x = 0.26$ has a T_c of only 2.4 K.

Figure 4 shows, in the main panel, the superconducting phase diagram of $\text{Na}_x\text{CoO}_2 \cdot \gamma\text{H}_2\text{O}$. The variation of T_c with x indicates that there is an optimal sodium composition for the occurrence of superconductivity, $x = 0.30$. T_c decreases at both lower and higher Na contents. As the sodium content increases between $x = 0.26$ and $x = 0.35$, the formal oxidation state of the Co decreases from 3.74+ to 3.65+, and the optimum for superconductivity is 3.70+. This variation of T_c with the degree of electronic doping of the CoO_2 planes, is analogous with the behaviour observed in the copper oxide superconductors. We note that the synthesis method we have employed, and other ambient temperature synthesis methods that might be used in this system, are likely to result in a distribution of sodium contents for each sample. If ideally uniform sodium content samples can be prepared, we expect that the superconducting ‘dome’ shown in Fig. 4 may become more narrow in sodium content.

Preliminary correlation of the chemical doping due to the Na content and the true electronic doping state of the CoO_2 planes can be accomplished by electron counting in the context of electronic pictures already being developed for both the dehydrated Na_xCoO_2 and $\text{Na}_x\text{CoO}_2 \cdot 1.3\text{H}_2\text{O}$ phases (see, for example, refs 4–9). For $x = 0$, the formal Co oxidation state is Co 4+, with a t_{2g}^5 electron configuration in the low spin state. For $x = 1$, Co is formally 3+, with an electron configuration of t_{2g}^6 in the low spin state. Electronic structure calculations for $\text{Na}_{0.5}\text{CoO}_2$ (ref. 6) indicate that the t_{2g} band would be completely filled at $x = 1$, and that an ‘ordinary’ semiconductor is expected. However, it has been pointed out that the trigonal distortion of the CoO_6 octahedra in these structures will probably lead to splitting of the t_{2g} band^{5,10}. The proposed t_{2g} band splitting would then, for $x = 0$, result in a fully filled four-electron band and a half-filled two-electron band, leading to the expectation that this compound will be a Mott–Hubbard insulator. $\text{Na}_x\text{CoO}_2 \cdot 1.3\text{H}_2\text{O}$ for $x = 0$ would then bear a striking similarity to La_2CuO_4 , the ground state for the copper oxide superconductors, where electrons at the Fermi energy also reside in a half-filled two-electron band. It has not yet been determined whether this half-filled state in the layered triangular lattice cobalt oxides at $x = 0$ gives rise to a Mott–Hubbard insulator as it does in the copper oxides. In this scenario, then, each added Na above $x = 0$ in $\text{Na}_x\text{CoO}_2 \cdot 1.3\text{H}_2\text{O}$ results in the addition of one electron per

cobalt to the half-filled band, and the optimal chemical doping level for superconductivity, $x = 0.3$, represents the addition of 0.3 electrons to the half-filled band per formula unit. Values of x less than 0.3 would then represent underdoped materials, and values of x greater than 0.3 would represent overdoped materials. More detailed characterization of the electronic state of the triangular cobalt oxides will be needed to determine just how closely the electronic analogies to the copper oxides hold.

This work reveals several experimental findings that are critical for understanding the superconductivity of $\text{Na}_x\text{CoO}_2 \cdot 1.3\text{H}_2\text{O}$. The discovery of a maximum in T_c as a function of the Na content establishes the optimal chemical doping level for superconductivity. A fundamental similarity between the layered copper oxide and layered cobalt oxide superconductors is seen in the decrease in T_c for both the underdoped and overdoped materials. The optimal doping level for superconductivity is clearly higher with respect to the Mott–Hubbard-like half-filled two-electron band in $\text{Na}_x\text{CoO}_2 \cdot 1.3\text{H}_2\text{O}$ (+0.3 electrons) than in the copper oxides (+0.15 electrons or holes). This may either reflect a fundamental difference between the two types of superconductors, or the influence of as-yet unknown structure–electronic state correlations in the cobalt oxides. Observations of unusual electrical transport properties in the host material $\text{Na}_{0.7}\text{CoO}_2$ itself suggest that coupled spin and charge dynamics may be implicated in the superconductivity, although there are significant differences from copper oxide systems^{10,11}. Observations that the lower hydrates with closer CoO_2 – CoO_2 interplanar distances are not superconducting above 2 K (ref. 2), and that T_c decreases under pressure¹², indicate that the two-dimensional character of the structure is important. Though the intrinsically complex materials chemistry of the $\text{Na}_x\text{CoO}_2 \cdot 1.3\text{H}_2\text{O}$ superconductor makes it difficult to characterize, we believe that potentially fruitful comparisons to the copper oxides, and the fact that this compound may represent the literal embodiment of Anderson’s original proposal for the resonating valence bond state¹³, make it worthy of further study. □

Received 6 June; accepted 2 July 2003; doi:10.1038/nature01877.

1. Takada, K. *et al.* Superconductivity in two-dimensional CoO_2 layers. *Nature* **422**, 53–55 (2003).
2. Foo, M. L. *et al.* Chemical instability of the cobalt oxyhydrate superconductor under ambient conditions. *Solid State Commun* **127**, 33–37 (2003).
3. Foussassier, C., Matjeka, G., Reau, J.-M. & Hagenmuller, P. Sur de nouveaux bronzes oxygènes de formule Na_xCoO_2 ($x \approx 1$). Le système cobalt-oxygène-sodium. *J. Solid State Chem.* **6**, 532–537 (1973).
4. Baskaran, G. An electronic model for CoO_2 layer based systems: Chiral RVB metal and superconductivity. Preprint at (<http://xxx.lanl.gov/cond-mat/0303649>) (2003).
5. Kumar, B. & Shastry, B. S. Superconductivity in CoO_2 layers and the resonating valence bond mean field theory of the triangular lattice t-J model. Preprint at (<http://xxx.lanl.gov/cond-mat/0304210>) (2003).
6. Singh, D. J. Electronic structure of NaCo_2O_4 . *Phys. Rev. B* **61**, 13397–13402 (2000).
7. Honercomp, C. Instabilities of interacting electrons on the triangular lattice. Preprint at (<http://xxx.lanl.gov/cond-mat/0304460>) (2003).
8. Tanaka, A. & Hu, X. Possible spin triplet superconductivity in $\text{Na}_x\text{CoO}_2 \cdot \gamma\text{H}_2\text{O}$. Preprint at (<http://xxx.lanl.gov/cond-mat/0304409>) (2003).
9. Wang, Q.-H., Lee, D.-H. & Lee, P. A. Doped t-J model on a triangular lattice: Possible application to $\text{Na}_x\text{CoO}_2 \cdot \gamma\text{H}_2\text{O}$ and Na_xTiO_2 . Preprint at (<http://xxx.lanl.gov/cond-mat/0304377>) (2003).
10. Terasaki, I., Sasago, Y. & Uchinokura, K. Large thermoelectric power in NaCo_2O_4 single crystals. *Phys. Rev. B* **56**, R12685–R12687 (1997).
11. Wang, Y., Rogado, N. S., Cava, R. J. & Ong, N. P. Spin entropy as the likely source of enhanced thermopower in NaCo_2O_4 . *Nature* **423**, 425–428 (2003).
12. Lorenz, B., Cmaidalka, J., Meng, R. L. & Chu, C. W. Effect of hydrostatic pressure on the superconductivity in $\text{Na}_x\text{CoO}_2 \cdot \gamma\text{H}_2\text{O}$. Preprint at (<http://xxx.lanl.gov/cond-mat/0304537>) (2003).
13. Anderson, P. W. Resonating valence bonds: A new type of insulator. *Mater. Res. Bull.* **8**, 153–160 (1973).

Acknowledgements This work was supported by the US National Science Foundation, Division of Materials Research, and the US Department of Energy, Division of Basic Energy Sciences. T.K. thanks the Foundation for Polish Science for support.

Competing interests statement The authors declare that they have no competing financial interests.

Correspondence and requests for materials should be addressed to R.J.C. (rcava@princeton.edu).